JACS
JOURNAL OF THE AMERICAN CHEMICAL SOCIETY

Communication

pubs.acs.org/JACS

Closed and Semiclosed Interhelical Structures in Membrane vs Closed and Open Structures in Detergent for the Influenza Virus Hemagglutinin Fusion Peptide and Correlation of Hydrophobic Surface Area with Fusion Catalysis

Ujjayini Ghosh, Li Xie, Lihui Jia, Shuang Liang, and David P. Weliky*

Department of Chemistry, Michigan State University, East Lansing, Michigan 48824, United States

Supporting Information

ABSTRACT: The ~25 N-terminal "HAfp" residues of the HA2 subunit of the influenza virus hemagglutinin protein are critical for fusion between the viral and endosomal membranes at low pH. Earlier studies of HAfp in detergent support (1) N-helix/turn/C-helix structure at pH 5 with open interhelical geometry and N-helix/turn/C-coil structure at pH 7; or (2) N-helix/turn/C-helix at both pHs with closed interhelical geometry. These different structures led to very different models of HAfp membrane location and different models of catalysis of membrane fusion by HAfp. In this study, the interhelical geometry of membrane-associated HAfp is probed by solid-state NMR. The data are well-fitted to a population mixture of closed and semiclosed structures. The two structures have similar interhelical geometries and are planar with hydrophobic and hydrophilic faces. The different structures of HAfp in detergent vs membrane could be due to the differences in interaction with the curved micelle vs flat membrane with better geometric matching between the closed and semiclosed structures and the membrane. The higher fusogenicity of longer sequences and low pH is correlated with hydrophobic surface area and consequent increased membrane perturbation.

Influenza virus is enveloped by a membrane which contains the hemagglutinin (HA) protein composed of the HA1 and HA2 subunits.[4] HA2 is a monotopic integral membrane protein, and HA1 is bound to the extraviral region of HA2. Infection of a host epithelial cell begins with HA1 binding to a cellular sialic acid receptor, and this binding triggers virion endocytosis. Endosomal pH is reduced to 5−6 via cell physiology, and deprotonation of HA2 acidic groups leads to refolding of HA2. The ~25 N-terminal "fusion peptide" (HAfp) residues of HA2 are highly conserved and important in fusion.[5] The HAfp becomes exposed after HA2 refolding and binds to a membrane.[6] Vesicle fusion is induced both by HAfp sequences as well as by larger HA2 constructs which include the HAfp, and there is greater fusion at acidic pH.[7] There have been several HAfp structures in detergent-rich media at different pH's and effort to correlate pH-dependent structural differences with membrane fusion.[1,2] However, there are large differences among the detergent structures so that structure/function correlation is unclear. The present work provides critical information about the HAfp structure in membrane. There are significant differences with the detergent structures, and the data support a role for HAfp hydrophobic surface area in fusion.

One structure/function model is based on the 20-residue HA3fp20 peptide (GLFGAIAGFIENGWEGMIDG) from the H3 viral subtype. The structures in detergent are N-helix/turn/C-helix at pH 5 and N-helix/turn/C-coil at pH 7.[1] The pH 5 structure is "open" as evidenced by the oblique interhelical angle (Figure 1A). EPR data were interpreted to support

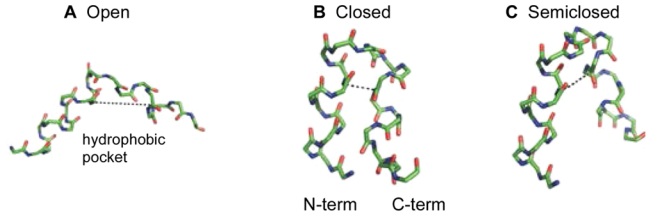

Figure 1. Backbone structural models of (A) open HA3fp20, (B) closed HA1fp23, and (C) semiclosed HA1fp23.[1−3] C, N, and O atoms are respectively represented by green, blue, and red vertices. The dashed lines are between F9 N and G16 CO with distances r_o = 11.5 Å, r_c = 3.9 Å, and r_s = 5.5 Å.

insertion of the N-helix to the membrane center at pH 5 with shallower insertion at pH 7. Relative to pH 7, greater fusion at pH 5 was explained by C-coil to C-helix change with formation of an open structure with a hydrophobic interhelical pocket and deep N-helix insertion. The pocket and insertion result in membrane perturbation and fusion.[8] A different fusion model was developed for the 23-residue HA1fp23 peptide (GLFGAIAGFIEGGWTGMIDGWYG) from the H1 viral subtype.[2] Relative to HA3fp20, HA1fp23 contains G12N, E15T, and additional WYG C-terminal residues. Unlike HA3fp20 which shows pH-dependent structure and open structure at pH 5, HA1fp23 has a "closed" N-helix/turn/C-helix structure in detergent at both pH 4 and 7 with tightly packed antiparallel N- and C-terminal helices (Figure 1B). Formation of closed HA1fp23 vs open HA3fp20 structure was attributed to the respective presence vs absence of C-terminal WYG.[9,10] The closed structure is amphipathic and would reasonably lie

Received: September 8, 2014
Published: June 3, 2015

DOI: 10.1021/jacs.5b04578
J. Am. Chem. Soc. 2015, 137, 7548−7551

on the membrane surface and potentially induce membrane perturbation. HA1fp23 in detergent at pH 4 also has a ~0.2 fraction of open structure with fast closed/open exchange.[11]

The different functional models are based on different structures in detergent and motivate the present work to understand the HAfp structure in membrane. HAfp induces fusion of membranes but not detergent micelles, so the membrane structures are more relevant for function. The present work builds on earlier solid-state NMR (SSNMR) studies of HA3fp20 in membranes showing N-helix/turn/C-helix structure at both pH 5 and 7, i.e., no C-coil structure at pH 7 as is found in detergent.[12] The structure was observed in both fluid- and gel-phase membranes. At pH 5, the interhelical separation of HA3fp20 in membrane is much less than for a HA3fp20 open structure in detergent.[3] The separation is consistent with a mixture of populations of closed structure and a somewhat different semiclosed structure, and therefore supports different HA3fp20 structures in membrane vs detergent (Figure 1C). Both the closed and semiclosed structures have a N-helix from residues 1−11 and C-helix from residues 14−22 and only differ in the residue 12/13 turn (Table S7).

The present study focuses on HA3fp20 and HA1fp23 in membrane: (1) to understand structural dependence on viral subtype amino acid differences, sequence length, and pH; and (2) to correlate structural features with fusion. Earlier work only showed N-helix/turn/C-helix structure for HA3fp20 in membrane at low and neutral pH, so the present work focuses on interhelical separation via rotational-echo double-resonance (REDOR) SSNMR measurement of the dipolar couplings (d's) of samples with labeled (*lab*) G16 ^{13}CO-F9 ^{15}N or A5 ^{13}CO-M17 ^{15}N spin pairs. The d depends on the ^{13}CO−^{15}N distance (r) as d(Hz) = 3066/r(Å)^3. A sample is at pH 5 (fusion pH in the endosome) or pH 7. A sample contains membrane-associated HA3fp20 or HA1fp23 with one labeling scheme (SI).[13,14] S_0 and S_1 ^{13}C REDOR spectra are acquired as a function of dephasing time (τ) and the S_0 and S_1 ^{13}CO intensities are used to calculate dephasing $\Delta S/S_0 = (S_0 - S_1)/S_0$ at each τ. For temperatures ≥0 °C, motion reduces $\Delta S/S_0$ and greatly complicates determination of r (Figure S7).[15] Temperature of −30 °C is therefore used to attenuate motion.

Figure 2 displays experimental spectra and $(\Delta S/S_0)^{exp}$ vs τ buildups. The G16 and A5 ^{13}CO peak shifts are respectively 177 and 179 ppm and correlate with helical structure.[2,12,16] The buildups reflect intra- rather than intermolecular spin pairs as evidenced by similar $(\Delta S/S_0)$ for samples with either all labeled or a 1:1 labeled:unlabeled mixture of HA3fp20 (Figure S3). For each labeling scheme, the $(\Delta S/S_0)^{exp}$ buildups are comparable for HA3fp20 and HA1fp23 samples at both pH's which support similar structures in all samples with minimal dependence on subtype sequence, pH, or the C-terminal WYG residues. Similar structures in membrane contrast with different open vs closed structures for HA3fp20 vs HA1fp23 in detergent at low pH. Additional insight is obtained from comparison with $(\Delta S/S_0)^{sim}$ vs τ in the closed, semiclosed, and open structures. In contrast to detergent, the open structure is never dominant in membrane.

The ^{13}CO intensities include dominant *lab* and minor natural abundance (*na*) signals with $(\Delta S/S_0)^{exp} = [f_{lab} \times (\Delta S/S_0)^{lab}] + [f_{na} \times (\Delta S/S_0)^{na}]$ and $f_{lab} \approx 0.75$ and $f_{na} \approx 0.25$. The most quantitative structural information is obtained from analysis of the $(\Delta S/S_0)^{lab}$, which is determined using the above equation and accurate estimates of $(\Delta S/S_0)^{na}$. The $(\Delta S/S_0)^{lab}$ is always

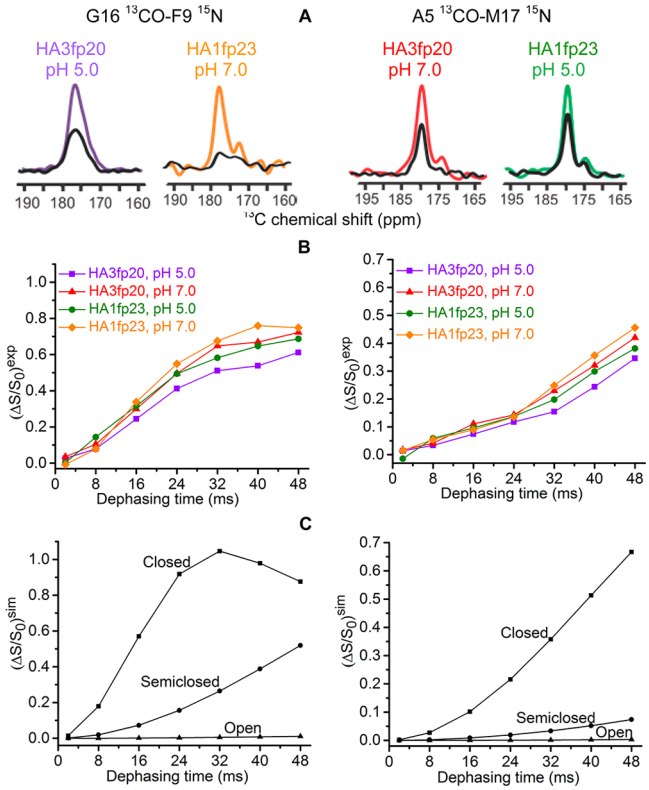

Figure 2. (A) ^{13}C-detect/^{15}N-dephase REDOR S_0 (colored) and S_1 (black) spectra for membrane-associated HAfp with 40 ms dephasing time. (B) Experimental and (C) simulated $(\Delta S/S_0)$ vs dephasing time.

close to the corresponding $(\Delta S/S_0)^{exp}$ with typical $(\Delta S/S_0)^{lab}/(\Delta S/S_0)^{exp} \approx 1.15$ (Tables S1 and S2). Each $(\Delta S/S_0)^{na}$ is an average over the ~25 different *na* sites, with the $(\Delta S/S_0)$ of each site calculated using the *na* ^{13}CO-*lab* ^{15}N distance of the closed structure (SI).

The $(\Delta S/S_0)^{lab}$ buildups do not quantitatively match the $(\Delta S/S_0)^{sim}$ buildups of the closed, semiclosed, or open structures. However, quantitative fitting is obtained for all buildups with a model for which a fraction (f_c) of the peptides in each sample type (sequence + pH) have closed structure and the remaining fraction (f_s) have semiclosed structure (Figure 3). In addition to the best-fit fractions shown in Figure 3, fitting includes best-fit r_{cG} = 3.9 Å and r_{sG} = 5.4 Å common to the four G16/F9 samples and best-fit r_{cA} = 5.4 Å and r_{sA} = 8.2 Å common to the four A5/M17 samples. These distances agree very well with the respective 3.9, 5.5, 5.4, and 8.2 Å values calculated from the closed HA1fp23 structure in detergent and the semiclosed HA3fp20 structure in membrane (Figure 1). The SI provides a full description of the fitting including best-fit parameter uncertainties and χ^2. Fitting is always worse with inclusion of an open structure population.

Significant differences between the structures in membrane vs detergent include: (1) presence vs absence of semiclosed structure; (2) absence vs presence of open structure; (3) mixture of closed and semiclosed structures for both HA3fp20 and HA1fp23 vs predominant open structure for HA3fp20 and closed structure for HA1fp23. The membrane and detergent samples are at thermodynamic equilibrium so the different structural populations reflect free energy differences between the two media. Some of these differences may be due to a locally flat membrane surface vs a locally curved detergent micelle surface (Figure 4). The closed and semiclosed

DOI: 10.1021/jacs.5b04578
J. Am. Chem. Soc. 2015, 137, 7548−7551

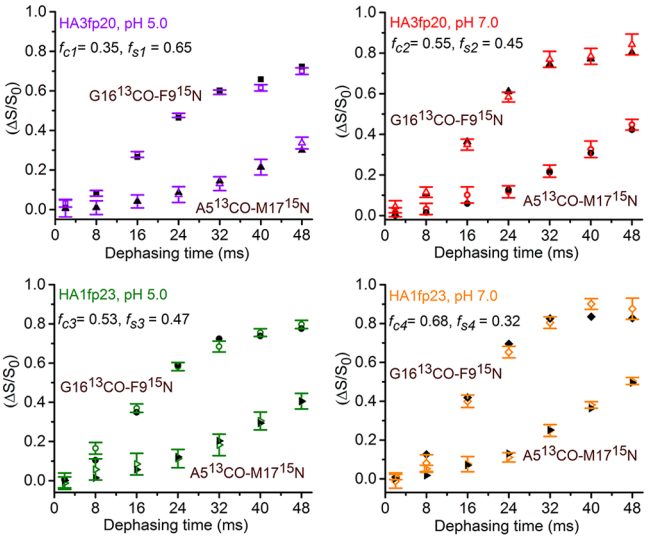

Figure 3. Plots of experimental $(\Delta S/S_0)^{lab}$ (colored) and best-fit $(\Delta S/S_0)^{sim}$ (black) from the closed/semiclosed model.

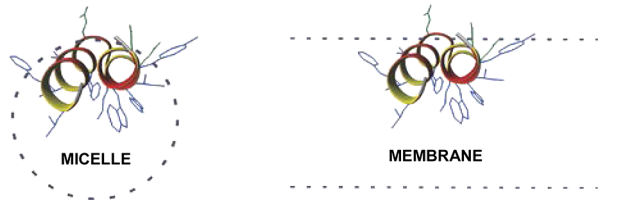

Figure 4. Models of detergent micelle and membrane locations of closed structure HA1fp23. Dashed lines are the hydrocarbon core.

structures are amphipathic with flat hydrophobic and hydrophilic surfaces on opposite faces that are geometrically matched to the surface of the amphipathic membrane. The presence of both closed and semiclosed structures in membrane may correlate to their similar hydrophobic surfaces and consequent similar protein/membrane interaction energies. There is less favorable matching with the curved micelle, particularly for the semiclosed structure which has more extended surfaces. The detergent micelle is also more plastic than the membrane with lower energy penalty for detergent relative to lipid relocation to shield the hydrophobic pocket of the open structure from water. For pH 7, there is good agreement between $f_c \approx 0.7$ for HA1fp23 in gel-phase membrane and $f_c \approx 1$ in bicelles with detergent:lipid ≈ 2:1 mole ratio.[17]

The similar closed and semiclosed populations in membrane reflect comparable free-energies of the two structures. Relative to HA3fp20, the larger f_c's of HA1fp23 may be due to stabilization of the tight N-helix/C-helix packing via the longer C-helix containing the additional WYG residues.[9,18] For either construct, larger f_c's at pH 7 and larger f_s's at pH 5 correlate with the protonation of E11 ($pK_a \approx 5.9$) adjacent to the turn.[19] Stabilization of the closed structure by E11 $-COO^-$ and the semiclosed structure by −COOH also correlates with the most stable structures observed in MD simulations of HA3fp20 in implicit membrane.[20] Computational energy minimization of the semiclosed structure resulted in retention of the semiclosed backbone and insertion of the F9 ring in the interhelical cavity (Figure 5A). This insertion is also observed in the MD structures with E11 −COOH. Insertion was probed by $^{13}CO-^{2}H$ REDOR of HA3fp20 with G16 ^{13}CO and F9 ring ^{2}H labeling (Figure 5B). There was greater buildup at pH 5

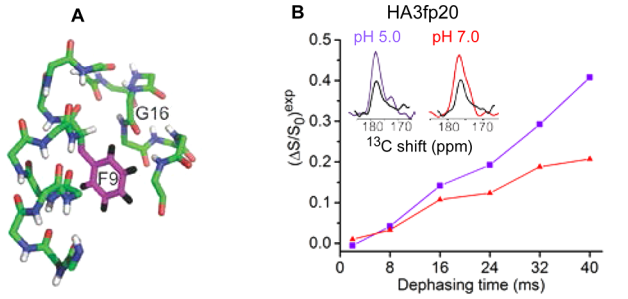

Figure 5. (A) Model of insertion of the F9 ring in the semiclosed structure. (B) ^{13}C-detect/^{2}H-dephase REDOR of HA3fp20 samples with G16 ^{13}CO/F9 ring ^{2}H labeling. The typical uncertainty is 0.02. S_0 (colored) and S_1 (black) spectra are for 40 ms dephasing time.

than pH 7, which correlates with (1) calculated G16 CO-F9 ring center distance of ∼5 Å in the semiclosed and ∼8 Å in the closed structure; and (2) a larger f_s in the pH 5 sample (Figure 3). The pH 5 buildup was well-fitted by a model with $f_c = 0.35$ and $f_s = 0.65$ and $^{13}CO-^{2}H$ $d_{cD} = 0$ and best-fit $d_{sD} = 19(1)$ Hz (Figure S8). This corresponds to $r_{sD} \approx 6$ Å and supports location of the F9 ring in the interhelical cavity of the semiclosed structure. There is also hydrophobic F9/M17 interaction (Figure S9).

Structure−function correlation was probed with assays of HAfp-induced vesicle fusion under the four sample conditions used for SSNMR (Figure 6A). Significant fusion is observed for

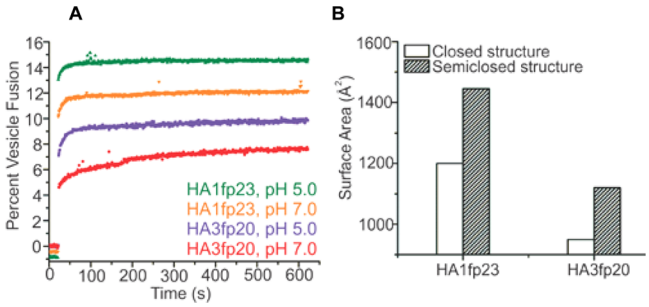

Figure 6. (A) HAfp-induced vesicle fusion for 1:50 peptide:lipid mole ratio. (B) Calculated HAfp hydrophobic surface areas.

all conditions, and the fusion extents are ordered (HA1fp23, pH 5) > (HA1fp23, pH 7) > (HA3fp20, pH 5) > (HA3fp20, pH 7), which is consistent with earlier work.[21] Relative to HA3fp20, the higher fusion of HA1fp23 supports a contribution from the C-terminal WYG residues. For either HA3fp20 or HA1fp23, there is higher fusion at pH 5 than pH 7 which correlates to larger f_s and smaller f_c at the lower pH and evidence higher fusion catalysis by the semiclosed structure. These data support a contribution to fusion catalysis from hydrophobic interaction between HAfp and the membrane (Figure 4). The mechanism is reduction in activation energy because the perturbed bilayer of the HAfp/membrane complex resembles the fusion transition state. The calculated HAfp hydrophobic surface area (S_a) is the quantity used to represent this hydrophobic interaction (Figure 6B). S_a(HA1fp23) > S_a(HA3fp20) because of the additional WYG residues, and S_a(semiclosed) > S_a(closed) because of the more open interhelical geometry of the semiclosed structure. The S_a of each sample is calculated using the experimentally derived f_c and f_s, and the ordering of these S_a's is the same as the fusion extents (Table S8). The S_a's and fusion extents for larger HA2

DOI: 10.1021/jacs.5b04578
J. Am. Chem. Soc. 2015, 137, 7548−7551

constructs also support the importance of protein hydrophobic surface area in fusion. One example is FHA2, the 185-residue extraviral domain of the HA2 subunit protein that includes HAfp.[7] The calculated S_a(FHA2):S_a(HA1fp23) ≈ 5 and FHA2 is a much better fusion catalyst than HA1fp23.[7]

Although most fusion peptide structures are in detergents, a structure in membrane is very important because fusion is induced between membranes but not micelles. The present and previous studies support substantial structural differences in membrane vs detergent. HAfp and fusion peptides from other viruses with very different sequences are α helical monomers in detergent and form α monomers as well as antiparallel β sheet oligomers in membrane.[15,22−24] The relative α and β populations are determined by membrane composition, e.g., inclusion of cholesterol often results in higher β population.[22,25] For the present study without cholesterol, both HA3fp20 and HA1fp23 are mixtures of closed and semiclosed α structures which are different than the dominant open HA3fp20 and closed HA1fp23 structures in detergent. Similar membrane fusion by HA3fp20 and HA1fp23 correlates much better with their similar structures in membrane than with their very different structures in detergent.

Previous studies on fusion induced by the full-length HA protein support the importance of the HAfp in catalyzing the early hemifusion (membrane joining) step of fusion.[26] Vesicle fusion resembles hemifusion, and HAfp-induced vesicle fusion is consistent with an important role for HAfp in hemifusion. The mixture of closed and semiclosed structures for HAfp in membrane is likely reflective of HAfp structure in full-length HA2 during virus/endosome fusion as evidenced by (1) the N-terminal 20- or 23-residue HAfp has autonomous folding in membrane, and the residue 34−175 C-terminal region has autonomous folding in aqueous solution; and (2) the HAfp and the residue 186−210 TM domain are the only HA regions which are deeply membrane-inserted after viral fusion.[6,27] HA is minimally trimeric, but the three HAfp helices do not contact one another in HA2 subunit ectodomain trimers.[28] HA2 probably contains α HAfp monomers at least during early hemifusion with the possibility of a second structural population of antiparallel β sheet oligomers.[22,29] HAfp fusion activity may also relate to large ratios of hydrophobic to hydrophilic surface areas. For HA3fp20, the ratio is 2.8 for closed and 4.2 for semiclosed structure, and for HA1fp23, the ratios are 2.4 and 3.7. Large ratios for amphipathic peptides are correlated to stabilization of negative membrane curvature which is a feature of fusion intermediates.[30,31] The semiclosed structures have the largest ratios so their greater fusogenicity may be due to curvature stabilization. The closed and semiclosed structures may also interconvert at ambient temperature with coupling to increased lipid motion and disorder which aid catalysis.[17]

■ ASSOCIATED CONTENT

Supporting Information

Additional descriptions of experimental procedures and data analysis and results. The Supporting Information is available free of charge on the ACS Publications website at DOI: 10.1021/jacs.5b04578.

■ AUTHOR INFORMATION

Corresponding Author

*weliky@chemistry.msu.edu

Notes

The authors declare no competing financial interest.

■ ACKNOWLEDGMENTS

This work was supported by NIH grant AI047153. NMR technical assistance was provided by Dr. Daniel Holmes.

■ REFERENCES

(1) Han, X.; Bushweller, J. H.; Cafiso, D. S.; Tamm, L. K. *Nat. Struct. Biol.* **2001**, *8*, 715.
(2) Lorieau, J. L.; Louis, J. M.; Bax, A. *Proc. Natl. Acad. Sci. U.S.A.* **2010**, *107*, 11341.
(3) Ghosh, U.; Xie, L.; Weliky, D. P. *J. Biomol. NMR* **2013**, *55*, 139.
(4) White, J. M.; Delos, S. E.; Brecher, M.; Schornberg, K. *Crit. Rev. Biochem. Mol. Biol.* **2008**, *43*, 189.
(5) Durell, S. R.; Martin, I.; Ruysschaert, J. M.; Shai, Y.; Blumenthal, R. *Mol. Membr. Biol.* **1997**, *14*, 97.
(6) Durrer, P.; Galli, C.; Hoenke, S.; Corti, C.; Gluck, R.; Vorherr, T.; Brunner, J. *J. Biol. Chem.* **1996**, *271*, 13417.
(7) Curtis-Fisk, J.; Preston, C.; Zheng, Z. X.; Worden, R. M.; Weliky, D. P. *J. Am. Chem. Soc.* **2007**, *129*, 11320.
(8) Lai, A. L.; Park, H.; White, J. M.; Tamm, L. K. *J. Biol. Chem.* **2006**, *281*, 5760.
(9) Lorieau, J. L.; Louis, J. M.; Bax, A. *Biopolymers* **2013**, *99*, 189.
(10) Du, T. P.; Jiang, L.; Liu, M. L. *J. Peptide Sci.* **2014**, *20*, 292.
(11) Lorieau, J. L.; Louis, J. M.; Schwieters, C. D.; Bax, A. *Proc. Natl. Acad. Sci. U.S.A.* **2012**, *109*, 19994.
(12) Sun, Y.; Weliky, D. P. *J. Am. Chem. Soc.* **2009**, *131*, 13228.
(13) Gullion, T.; Schaefer, J. *J. Magn. Reson.* **1989**, *81*, 196.
(14) Cegelski, L. *Bioorg. Med. Chem. Lett.* **2013**, *23*, 5767.
(15) Bodner, M. L.; Gabrys, C. M.; Parkanzky, P. D.; Yang, J.; Duskin, C. A.; Weliky, D. P. *Magn. Reson. Chem.* **2004**, *42*, 187.
(16) Zhang, H. Y.; Neal, S.; Wishart, D. S. *J. Biomol. NMR* **2003**, *25*, 173.
(17) Lorieau, J. L.; Louis, J. M.; Bax, A. *J. Am. Chem. Soc.* **2011**, *133*, 14184.
(18) Lorieau, J. L.; Louis, J. M.; Bax, A. *J. Am. Chem. Soc.* **2011**, *133*, 2824.
(19) Chang, D. K.; Cheng, S. F.; Lin, C. H.; Kantchev, E. A. B.; Wu, C. W. *Biochim. Biophys. Acta* **2005**, *1712*, 37.
(20) Panahi, A.; Feig, M. *J. Phys. Chem. B* **2010**, *114*, 1407.
(21) Wharton, S. A.; Martin, S. R.; Ruigrok, R. W. H.; Skehel, J. J.; Wiley, D. C. *J. Gen. Virol.* **1988**, *69*, 1847.
(22) Yang, J.; Parkanzky, P. D.; Bodner, M. L.; Duskin, C. G.; Weliky, D. P. *J. Magn. Reson.* **2002**, *159*, 101.
(23) Yao, H. W.; Hong, M. *J. Mol. Biol.* **2013**, *425*, 563.
(24) Apellaniz, B.; Huarte, N.; Largo, E.; Nieva, J. L. *Chem. Phys. Lipids* **2014**, *181*, 40.
(25) Qiang, W.; Weliky, D. P. *Biochemistry* **2009**, *48*, 289.
(26) Kemble, G. W.; Danieli, T.; White, J. M. *Cell* **1994**, *76*, 383.
(27) Chen, J.; Skehel, J. J.; Wiley, D. C. *Proc. Natl. Acad. Sci. U.S.A.* **1999**, *96*, 8967.
(28) Macosko, J. C.; Kim, C. H.; Shin, Y. K. *J. Mol. Biol.* **1997**, *267*, 1139.
(29) Schmick, S. D.; Weliky, D. P. *Biochemistry* **2010**, *49*, 10623.
(30) Tytler, E. M.; Segrest, J. P.; Epand, R. M.; Nie, S. Q.; Epand, R. F.; Mishra, V. K.; Venkatachalapathi, Y. V.; Anantharamaiah, G. M. *J. Biol. Chem.* **1993**, *268*, 22112.
(31) Smrt, S. T.; Draney, A. W.; Lorieau, J. L. *J. Biol. Chem.* **2015**, *290*, 228.

DOI: 10.1021/jacs.5b04578
J. Am. Chem. Soc. 2015, 137, 7548−7551

SUPPORTING INFORMATION

"Closed and semiclosed interhelical structures in membrane vs closed and open structures in detergent for the influenza virus hemagglutinin fusion peptide and correlation of hydrophobic surface area with fusion catalysis" by Ujjayini Ghosh, Li Xie, Lihui Jia, Shuang Liang, and David P. Weliky

1. Reagents. Protected amino acids and resins were obtained from Novabiochem, Sigma-Aldrich, and DuPont, and lipids were obtained from Avanti Polar Lipids. 1-^{13}C Gly and ^{15}N-Phe were obtained from Cambridge Isotopes and then *N*-Fmoc- or *N*-*t*-Boc-protected in our laboratory.[1,2] Other reagents were typically obtained from Sigma-Aldrich.

2. Peptide sequences.

HA3fp20: GLFGAIAGFIENGWEGMIDGGGKKKKG.

HA1fp23: GLFGAIAGFIEGGWTGMIDGWYGGGKKKKG

The underlined residues are *N*-terminal regions of the HA2 subunit of the hemagglutinin protein of influenza A virus. HA3fp20 and HA1fp23 are chosen because their structures have been extensively characterized in detergent micelles and detergent-rich bicelles. These structures are very different from one another and are predominantly open (HA3fp20) and closed (HA1fp23). The HA3fp20 and HA1fp23 sequences are respectively from the H3 and H1 viral subtypes with sequence variations N12/G12 and E15/T15. Shaded residues 21-23 (WYG) are conserved in both subtypes and are included in HA1fp23 but not HA3fp20. Both peptides have a non-native *C*-terminal GGKKKKG tag that greatly increases aqueous solubility needed both for peptide purification and for NMR sample preparation.

3. Peptide preparation. HA3fp20 was successfully made with manual Fmoc solid-phase synthesis whereas HA1fp23 could be made with manual *t*-Boc but not Fmoc synthesis. HF

cleavage after *t*-Boc synthesis was done by Midwest Bio-Tech. Purification was done by reversed-phase HPLC with a C18 column and resulted in >95% peptide purity as estimated from MALDI mass spectra. Peptide concentrations were quantitated with A_{280} and ε=5700 $cm^{-1}M^{-1}$ (HA3fp20) and ε=12660 $cm^{-1}M^{-1}$ (HA1fp23). The typical purified yield was ~10 μmole peptide per 200 μmole resin. Each peptide was either labeled with: G16-^{13}CO, F9-^{15}N; A5-^{13}CO, M17-^{15}N; or G16-^{13}CO, F9 ring-^{2}H (5 sites).

4. Lipids. Ether- rather than ester-linked lipids were used because they lack carbonyl (CO) carbons and therefore do not contribute natural abundance (*na*) ^{13}CO signal to the solid-state NMR (SSNMR) spectrum. The lipids were 1,2-di-*O*-tetradecyl-*sn*-glycero-3-phosphocholine (DTPC) and 1,2-di-*O*-tetradecyl-*sn*-glycero-3-[phosphor-*rac*-(1-glycerol)] (DTPG). A DTPC: DTPG (4:1) composition reflects the large fraction of phosphatidylcholine lipid in the membranes of the respiratory epithelial cells infected by influenza virus and the negative charge of these membranes.[3] Membrane binding of the cationic peptide was also enhanced by the negative charge.

5. Vesicle preparation. Lipids were dissolved in chloroform:methanol (9:1) and solvent was removed by nitrogen gas followed by vacuum pumping overnight. The lipid film was suspended in aqueous buffer (10 mM HEPES/5 mM MES/0.01% w/v NaN_3) and homogenized with freeze/thaw cycles. Unilamellar vesicles were made by repeated extrusion through a polycarbonate filter with a 100 nm diameter pores.

6. Vesicle fusion assay.[4] "Unlabeled" vesicles were prepared as above. "Labeled" vesicles were similarly prepared and contained an additional 2 mole% fluorescent lipid and 2 mole% quenching lipid, respectively *N*-(7-nitro-2,1,3-benzoxadiazol-4-yl) (ammonium salt) dipalmitoylphosphatidylethanolamine (*N*-NBD-DPPE) and *N*-(lissaminerhodamine B sulfonyl)

(ammonium salt) dipalmitoylphosphatidylethanolamine (N-Rh-DPPE). Labeled and unlabeled vesicles were mixed in 1:9 ratio and the temperature was maintained at 37 ^{o}C. The initial vesicle fluorescence (F_0) was measured, an aliquot of peptide stock was then added, and the time-dependent fluorescence $F(t)$ was subsequently measured in 1 s increments for a total time of 10 min. Peptide-induced fusion between labeled and unlabeled vesicles increased the average fluorophore-quencher distance and resulted in higher fluorescence. An aliquot of Triton X-100 detergent stock was then added and solubilized the vesicles with resultant further increase in the fluorophore-quencher distance and maximal fluorescence, F_{max}. The percent vesicle fusion was calculated as $M(t) = \{[F(t) - F_0] \times 100\}/\{[F_{max} - F_0]\}$. There was typically <2% variation in long-time $M(t)$ among assay replicates. Experimental conditions typically included: (1) initial 1500 μL vesicle suspension with [total lipid] = 150 μM; (2) 467 nm excitation and 530 nm detection wavelengths; (3) 90 μL aliquot of 50 μM peptide stock in water with final [peptide] = 3 μM and peptide:lipid mole ratio = 1:50; (4) 4 s assay dead-time after peptide addition; and (5) 12 μL aliquot of 20% v/v Triton X-100 with final 0.19% v/v Triton X-100.

7. Solid-state NMR sample preparation. Stock peptide solution (0.2 mM) was added dropwise to vesicle suspensions while maintaining the pH at either 5.0 or 7.0. The final peptide:lipid mole ratio =1:25. The suspension was gently vortexed overnight and then ultracentrifuged at 100000*g* for four hours. The membrane pellet with bound peptide was packed in a 4 mm diameter magic angle spinning (MAS) rotor. There was quantitative binding of the peptide to the membrane as evidenced by $A_{280} < 0.01$ in the supernatant.

8. Solid-state NMR (SSNMR). Spectra were acquired with a 9.4 T Agilent Infinity Plus spectrometer and triple-resonance MAS probe tuned to ^{1}H, ^{13}C, and ^{15}N frequencies or ^{1}H, ^{13}C, and ^{2}H frequencies. The sample rotor was cooled with nitrogen gas at –50 °C and the expected

sample temperature is ~ –30 °C. The REDOR pulse sequence was in time-sequence: (1) a ^{1}H $\pi/2$ pulse; (2) ^{1}H to ^{13}C cross-polarization (CP); (3) dephasing period of variable duration τ; and (4) ^{13}C detection.[5,6] ^{1}H decoupling was applied the dephasing and detection periods. There was interleaved acquisition of the S_0 and S_1 data. The dephasing periods of both acquisitions included a ^{13}C π-pulse at the end of each rotor cycle except the last cycle and the dephasing period of the S_1 acquisition included an additional ^{15}N π-pulse or ^{2}H π-pulse at the midpoint of each cycle. For the S_0 acquisition, there was no net ^{13}C evolution due to ^{13}C-^{15}N or ^{13}C-^{2}H dipolar coupling over a full rotor cycle. For the S_1 acquisition, there was net evolution with consequent reduction in the ^{13}C signal. Typical NMR parameters included 10 kHz MAS frequency, 5.0 μs ^{1}H $\pi/2$-pulse, 50 kHz ^{1}H CP, 60–65 kHz ramped ^{13}C CP, 80 kHz ^{1}H decoupling, and 8.1 μs ^{13}C, 10.0 μs ^{15}N, and 5.0 μs ^{2}H π-pulses with XY-8 phase cycling applied to both pulse trains.[7] Spectra were typically processed using 100 Hz Gaussian line broadening and baseline correction. The S_0^{exp} and S_1^{exp} intensities were determined from integration of 3 ppm windows centered at the peak ^{13}CO shift. The uncertainties were the RMSD's of spectral noise regions with 3-ppm widths. Spectra were externally referenced to adamantane and assignment of the methylene peak to 40.5 ppm ^{13}C shift allowed direct comparison with liquid-state ^{13}C shifts.[8] Fig. S1 displays the entire shift region of one of the G16/F9 spectra in the absence and presence of baseline correction. In the absence of baseline correction, the typical period of oscillation in the baseline is ~200 ppm which is much larger than the typical full-width-at-half-maximum linewidth of ~5 ppm of a ^{13}CO peak. The ^{13}CO T_1 > 100 s which is typical for organic solids without large-amplitude motions.

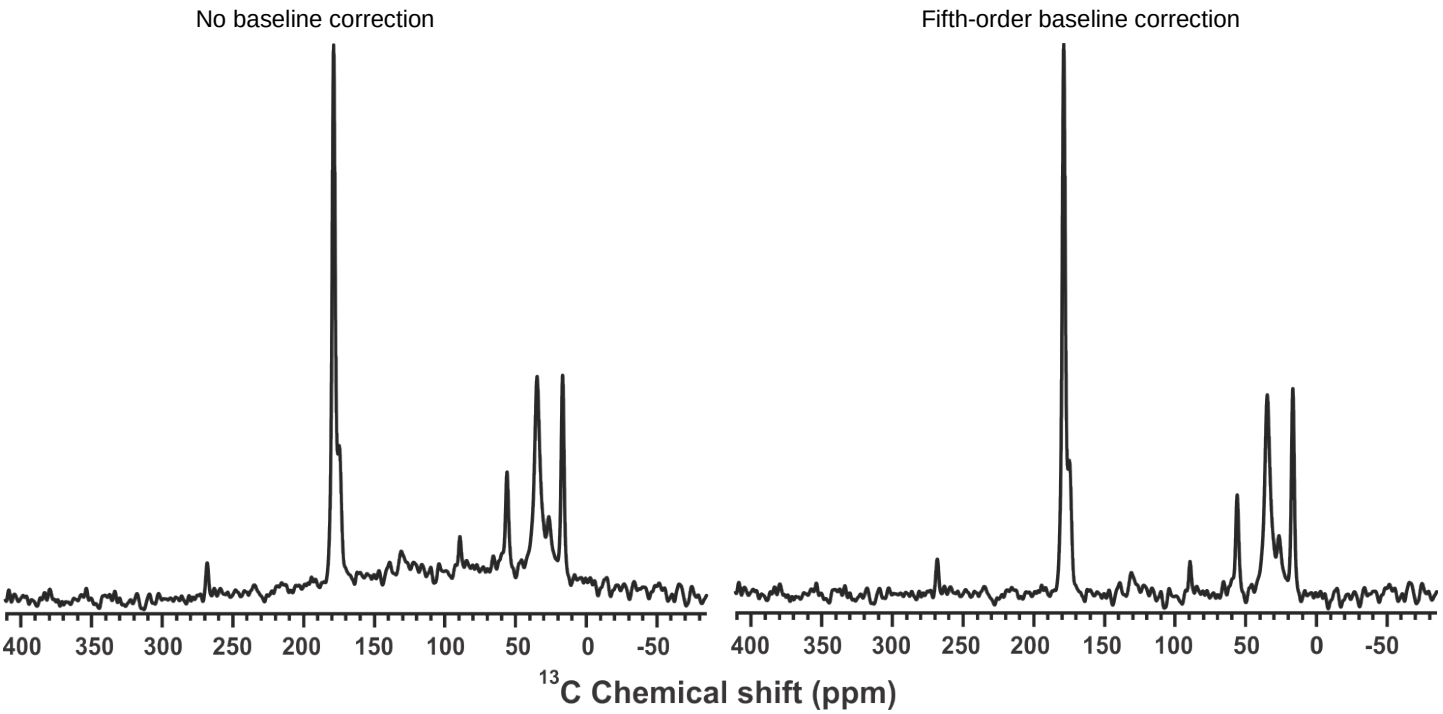

Figure S1. τ = 2 ms S_0 REDOR spectrum of the HA1fp23 pH 7.0 sample (left) without baseline correction and (right) with 5^{th}-order baseline correction.

9. Calculation of $(\Delta S/S_0)^{lab}$. Quantitative analysis of ^{13}CO-^{15}N REDOR includes determination of the $(\Delta S/S_0)^{lab}$ and $(\Delta S/S_0)^{na}$ contributions to $(\Delta S/S_0)^{exp}$ from the labeled (*lab*) and natural abundance (*na*) ^{13}CO nuclei. A $S_0{}^{lab}$= 0.99 contribution is estimated from the fractional labeling and $S_0{}^{na} = N\times0.011$ is estimated for N unlabeled (*unlab*) ^{13}CO sites which contribute to the $S_0{}^{exp}$ signal. The value of N is not precisely known because the individual spectra of some of the *unlab* sites will not completely overlap with the dominant *lab* spectrum used to set the 3 ppm integration window for $S_0{}^{lab}$.[9] We approximate that all the backbone and none of the sidechain ^{13}CO sites contribute to $S_0{}^{exp}$ so that N = 26 for HA3fp20 and N = 29 for HA1fp23. The calculated $(\Delta S/S_0)^{lab}$ is typically <10% different than the corresponding $(\Delta S/S_0)^{exp}$ and is not strongly dependent on the precise value of N (Table S2). The derivation of $(\Delta S/S_0)^{lab}$:

$$S_0^{exp} = S^{lab}_0 + S_0^{na} = 0.99 + 0.011\times N \qquad \text{-S1}$$

$$S_1^{exp} = S^{lab}_1 + S_1^{na} = S_1^{lab} + \sum_{k=1}^{N} S_{1k} \qquad \text{-S2}$$

For each unlabeled backbone site, $S_0{}^{na}$= 0.011:

$$(\frac{\Delta S}{S_0})^{na} = (\frac{S_0^{na} - S_1^{na}}{S_0^{na}}) = \frac{0.011 - S_1^{na}}{0.011} \qquad \text{-S3a}$$

$$S_1^{na} = 0.011 - 0.011\times(\frac{\Delta S}{S_0})^{na} \qquad \text{-S3b}$$

Summing over all *unlab* sites:

$$\sum_{k=1}^{N} S_{1k}^{na} = \sum_{k=1}^{N}\{0.011 - 0.011\times(\frac{\Delta S}{S_0})_k^{unlab}\} = 0.011\times N - 0.011\times\sum_{k=1}^{N}(\frac{\Delta S}{S_0})_k^{unlab} \qquad \text{-S4}$$

Substituting Eq. S4 into Eq. S2:

$$S_1^{exp} = S_1^{lab} + 0.011\times N - 0.011\times\sum_{k=1}^{N}(\frac{\Delta S}{S_0})_k^{unlab} \qquad \text{-S5}$$

Combining Eqs. S1, S2, and S5 followed by algebra:

-S6

$$(\frac{\Delta S}{S_0})^{exp} = \frac{S_0^{exp} - S_1^{exp}}{S_0^{exp}} = \frac{0.99 - S_1^{lab} + 0.011 \times \sum_{k=1}^{26} (\frac{\Delta S}{S_0})_k^{unlab}}{1.276}$$

Rearranging Eq. S6:

$$(\frac{\Delta S}{S_0})^{lab} = \frac{0.99 + 0.011 \times N}{0.99} \times (\frac{\Delta S}{S_0})^{exp} - 0.011 \times \sum_{k=1}^{N} (\frac{\Delta S}{S_0})_k^{unlab}$$

with $(\frac{\Delta S}{S_0})^{na} = 0.011 \times \sum_{k=1}^{N} (\frac{\Delta S}{S_0})_k^{unlab}$ -S8

For HA3fp20:

$$(\frac{\Delta S}{S_0})^{lab} = 1.2889 \times (\frac{\Delta S}{S_0})^{exp} - 0.011 \times \sum_{k=1}^{26} (\frac{\Delta S}{S_0})_k^{na}$$ -S9

For HA1fp23:

$$(\frac{\Delta S}{S_0})^{lab} = 1.3222 \times (\frac{\Delta S}{S_0})^{exp} - 0.011 \times \sum_{k=1}^{29} (\frac{\Delta S}{S_0})_k^{na}$$ -S10

Each of the $(\Delta S/S_0)_k^{unlab}$ was calculated using the $^{13}CO_k$ – F9 ^{15}N or the $^{13}CO_k$ – M17 ^{15}N separation ≡ r_k, the corresponding dipolar coupling d_k (Hz) = {3066/[r_k (Å)]^3}, and the quantum-

Table S1. ($\Delta S/S_0$) values for the G16 ^{13}CO/F9 ^{15}N samples[a]

τ	HA3fp20					HA1fp23			
(ms)	pH 5.0		pH 7.0			pH 5.0		pH 7.0	
	$(\Delta S/S_0)^{exp}$	$(\Delta S/S_0)^{lab}$	$(\Delta S/S_0)^{exp}$	$(\Delta S/S_0)^{lab}$	$(\Delta S/S_0)^{na}$	$(\Delta S/S_0)^{exp}$	$(\Delta S/S_0)^{lab}$	$(\Delta S/S_0)^{exp}$	$(\Delta S/S_0)^{lab}$
2	0.026(15)	0.032(19)	0.036(23)	0.044(29)	0.002	0.003(29)	0.001(38)	-0.008(28)	-0.012(36)
8	0.079(11)	0.082(15)	0.105(19)	0.115(25)	0.019	0.144(23)	0.167(30)	0.078(33)	0.082(43)
16	0.244(11)	0.278(15)	0.299(21)	0.349(27)	0.037	0.316(17)	0.374(22)	0.338(25)	0.403(32)
24	0.412(8)	0.476(11)	0.495(19)	0.583(24)	0.055	0.494(16)	0.588(21)	0.549(23)	0.659(29)
32	0.511(8)	0.593(11)	0.648(31)	0.769(39)	0.066	0.582(22)	0.691(28)	0.676(23)	0.812(30)
40	0.538(12)	0.616(16)	0.669(30)	0.784(39)	0.078	0.647(15)	0.763(19)	0.759(21)	0.909(28)
48	0.612(13)	0.699(17)	0.723(40)	0.843(52)	0.089	0.687(16)	0.805(21)	0.749(42)	0.884(55)

[a] The calculated $(\Delta S/S_0)^{na}$ are the same for all samples.

Table S2. ($\Delta S/S_0$) values for the A5 ^{13}CO/M17 ^{15}N samples[a]

τ	HA3fp20					HA1fp23			
(ms)	pH 5.0		pH 7.0			pH 5.0		pH 7.0	
	$(\Delta S/S_0)^{exp}$	$(\Delta S/S_0)^{lab}$	$(\Delta S/S_0)^{exp}$	$(\Delta S/S_0)^{lab}$	$(\Delta S/S_0)^{na}$	$(\Delta S/S_0)^{exp}$	$(\Delta S/S_0)^{lab}$	$(\Delta S/S_0)^{exp}$	$(\Delta S/S_0)^{lab}$
2	0.014(33)	0.012(43)	0.017(17)	0.016(22)	0.006	–0.014(24)	–0.013(32)	0.015(13)	0.014(17)
8	0.034(26)	0.023(34)	0.041(21)	0.033(27)	0.021	0.059(41)	0.057(55)	0.055(14)	0.052(18)
16	0.074(25)	0.054(32)	0.111(30)	0.102(39)	0.042	0.096(42)	0.085(56)	0.089(30)	0.076(40)
24	0.117(31)	0.084(40)	0.143(22)	0.117(29)	0.068	0.137(36)	0.113(47)	0.136(18)	0.111(24)
32	0.154(27)	0.121(35)	0.229(23)	0.219(29)	0.079	0.198(42)	0.183(56)	0.248(23)	0.249(31)
40	0.244(30)	0.227(39)	0.320(31)	0.327(40)	0.090	0.299(35)	0.305(46)	0.356(12)	0.381(17)
48	0.346(23)	0.351(29)	0.419(20)	0.448(26)	0.098	0.381(30)	0.406(40)	0.456(14)	0.504(18)

[a] The calculated $(\Delta S/S_0)^{na}$ are the same for all samples.

mechanically-derived expression for a pair of coupled spin ½ heteronuclei:

$$(\frac{\Delta S}{S_0})^{sim}\{d,\tau\} = 1 - [J_0(\sqrt{2}\lambda)]^2 + \{2 \times \sum_{k=1}^{5} \frac{[J_k(\sqrt{2}\lambda)]^2}{16k^2 - 1}\} \qquad \text{-S11}$$

with $\lambda = d \times \tau$, $\tau \equiv$ duration of the dephasing period, and $J_k \equiv k^{th}$-order Bessel function of the first kind.[10] This is a reasonable approach to r_k estimation because all the $(\Delta S/S_0)^{lab}$ buildups are well-fitted by mixtures of molecules with either closed or semiclosed structure. Tables S1 and S2 list the $(\Delta S/S_0)^{exp}$, $(\Delta S/S_0)^{lab}$, and $(\Delta S/S_0)^{na}$ for the eight data sets.

10. Intermolecular vs Intramolecular G16 ^{13}CO-F9 ^{15}N proximity. Close intermolecular proximity [G16 ^{13}CO (molecule 1) to F9 ^{15}N (molecule 2)] is possible if there are large populations of dimers or higher-order oligomers. This proximity was probed by comparison of the $\Delta S/S_0$ buildups between HA3fp20 samples prepared with either 2 μmole labeled HA3fp20 or 1 μmole labeled and 1 μmole unlabeled HA3fp20 (Fig. S3). Dominant intermolecular proximity would result in $(\Delta S/S_0)^{mixed}/(\Delta S/S_0)^{fully\ lab} < 1$ and dominant intramolecular proximity would result

in $(\Delta S/S_0)^{mixed}/(\Delta S/S_0)^{fully\ lab} \approx 1$. The latter result is observed with much better agreement of $(\Delta S/S_0)^{mixed}$ with calculated $(\Delta S/S_0)^{intra}$ than with calculated $(\Delta S/S_0)^{inter}$.

Derivation of $(\Delta S/S_0)^{inter}$. Fig. S2 displays an antisymmetric dimer model with the three possible configurations for a mixture containing p_L fraction labeled peptide and $(1–p_L)$ fraction unlabeled peptide: (**i**) both labeled with fractional population p_L^2; (**ii**) one labeled and one unlabeled with population $[2 \times p_L \times (1–p_L)]$; and (**iii**) both unlabeled with population $(1 – p_L)^2$.

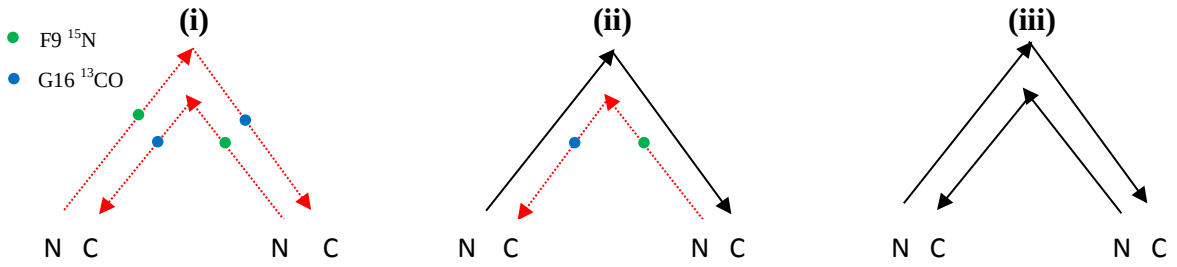

Figure S2. Anti-symmetric dimer configurations of HAfp. Each arrow represents either *N*- or *C*- terminal helices. Labeled HAfp is a red dashed line and unlabeled HAfp is a black line.

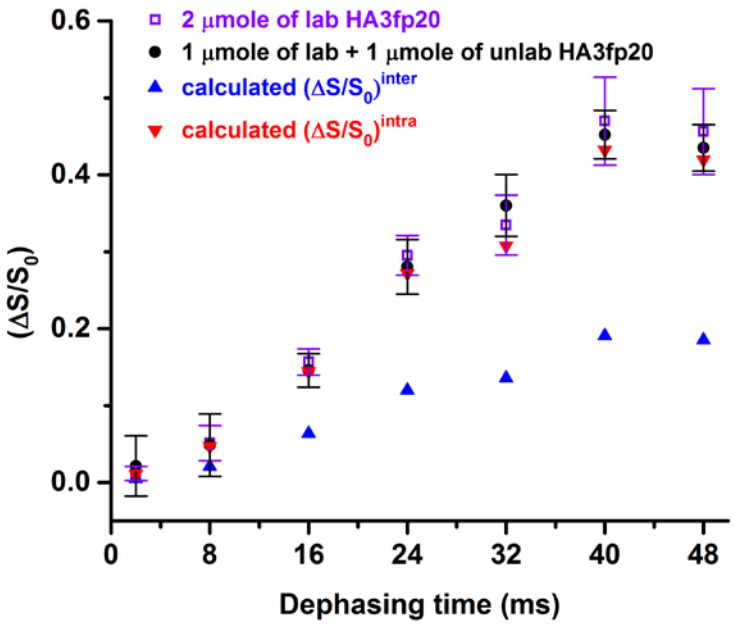

Figure S3. $(\Delta S/S_0)^{exp}$ buildups for pH 5 samples with either 2 μmole G16 ^{13}CO/F9 ^{15}N labeled HA3fp20 or 1 μmole labeled and 1 μmole unlabeled HA3fp20. The calculated $(\Delta S/S_0)^{intra}$ and $(\Delta S/S_0)^{inter}$ for the mixed sample are also displayed.

Table S3. S_0 expressions for intermolecular and intramolecular models [a]

	Intermolecular model			Intramolecular model
	Configuration **i**	Configuration **ii**	Configuration **iii**	
S_0^{lab}	$2p_L^2$	$2p_L \times (1-p_L)$	0	p_L
S_0^{na}	$p_L^2 \times 2N \times 0.011$	$2p_L \times (1-p_L) \times (2N+1) \times 0.011$	$(1-p_L^2) \times 2(N+1) \times 0.011$	$(N+1-p_L) \times 0.011$

[a] $N+1 \equiv$ number of residues in peptide.

The model includes:

1. All labeled molecules contain G16 ^{13}CO and F9 ^{15}N *lab* nuclei. The experimental fractional labeling is 0.99 and the approximation of 1.0 simplifies the calculations.

2. There is G16 ^{13}CO-F9 ^{15}N proximity for both *lab* spin pairs molecules in configuration **i**. Similar results are also obtained for one proximal and one distant *lab* spin pair.

3. There isn't ^{13}CO-^{15}N proximity for *lab* ^{13}CO nuclei in configuration **ii** or *na* ^{13}CO nuclei in all configurations. The consequent approximation $S_1 = S_0$ simplifies the calculations.

Table S3 summarizes the calculated S_0^{lab} and S_0^{na} contributions.

$$S_0^{inter} = S_0^{lab} + S_0^{na} \quad \text{-S12}$$

$$S_1^{inter} = S_1^{lab} + S_1^{na} \quad \text{-S13}$$

The only significant contribution to $(\Delta S/S_0)^{inter}$ are from *lab* spin pairs of configuration **i** and are denoted $(\Delta S/S_0)^{lab,i}$. For HA3fp20 with $N+1=27$, algebraic manipulation results in:

$$\left(\frac{\Delta S}{S_0}\right)^{inter} = \frac{2.00\left(\frac{\Delta S}{S_0}\right)^{lab,i}}{2.57\,p_L^2 + 3.17\,p_L(1-p_L) + 0.59\,(1-p_L)^2} \quad \text{-S14}$$

When $p_L = 1.0$:

$$\left(\frac{\Delta S}{S_0}\right)^{inter}_{p_L=1.0} = 0.778 \times \left(\frac{\Delta S}{S_0}\right)^{lab,i} \quad \text{-S15}$$

When $p_L = 0.5$:

$$(\frac{\Delta S}{S_0})^{inter}_{p_L=0.5} = 0.316 \times (\frac{\Delta S}{S_0})^{lab,i} \quad \text{-S16}$$

The blue up triangles in Fig. S3 are calculated:

$$(\frac{\Delta S}{S_0})^{inter}_{p_L=0.5} = 0.316 \times (\frac{\Delta S}{S_0})^{lab,i} = \frac{0.316}{0.778} \times (\frac{\Delta S}{S_0})^{lab,i}_{p_L=1.0} = 0.406 \times (\frac{\Delta S}{S_0})^{exp}_{p_L=1.0} \quad \text{-S17}$$

An alternate dimer structure was also considered in which configuration **i** contains one *lab* pair with close proximity as well as one *lab* pair with distant proximity and S_1=S_0:

$$(\frac{\Delta S}{S_0})^{inter}_{p_L=0.5} = 0.158 \times (\frac{\Delta S}{S_0})^{lab,i} = \frac{0.158}{0.389} \times (\frac{\Delta S}{S_0})^{lab,i}_{p_L=1.0} = 0.406 \times (\frac{\Delta S}{S_0})^{exp}_{p_L=1.0} \quad \text{-S18}$$

Relative to a dimer structure with both *lab* pairs in close proximity, the ($\Delta S/S_0$) values are smaller for a structure with one *lab* pair in close proximity. However, the (p_L=0.5)/(p_L=1.0) ratio = 0.41 remains the same for either dimer structure.

Derivation of $(\Delta S/S_0)^{intra}$. The model includes: (1) every labeled peptide contains a *lab*^{13}CO-^{15}N pair in close intramolecular but not intermolecular proximity; and (2) S_1^{na}=S_0^{na}.

$$S_0^{intra} = S_0^{lab} + S_0^{na} \quad \text{-S19}$$

$$S_1^{intra} = S_1^{lab} + S_1^{na} \quad \text{-S20}$$

The expressions from Table S3 and algebraic manipulation with N+1=27 result in:

$$(\frac{\Delta S}{S_0})^{intra} = \frac{p_L \times (\frac{\Delta S}{S_0})^{lab}}{p_L + 0.286} \quad \text{-S21}$$

For p_L = 1.0, the result is the same as the intermolecular model:

$$(\frac{\Delta S}{S_0})^{intra}_{p_L=1.0} = 0.778 \times (\frac{\Delta S}{S_0})^{lab} \quad \text{-S22}$$

For p_L = 0.5:

$$(\frac{\Delta S}{S_0})^{intra}_{p_L=0.5} = 0.636 \times (\frac{\Delta S}{S_0})^{lab} \quad \text{-S23}$$

The red down triangles in Fig. S3 are calculated:

$$(\frac{\Delta S}{S_0})^{intra}_{p_L=0.5} = 0.636 \times (\frac{\Delta S}{S_0})^{lab} = \frac{0.636}{0.778} \times (\frac{\Delta S}{S_0})^{lab}_{p_L=1.0} = 0.818 \times (\frac{\Delta S}{S_0})^{exp}_{p_L=1.0} \quad \text{-S24}$$

Eqs.S17 and S24 show that decreasing p_L results in much greater reduction of $(\Delta S/S_0)^{inter}$ than $(\Delta S/S_0)^{intra}$. There is much better agreement of $(\Delta S/S_0)^{exp}{}_{pL=0.5}$ with $(\Delta S/S_0)^{intra}{}_{pL=0.5}$ than with $(\Delta S/S_0)^{inter}{}_{pL=0.5}$ (Fig. S3).

11. Fitting of the ^{13}CO-^{15}N REDOR data with the closed/semiclosed model

The experimentally-derived $(\Delta S/S_0)^{lab}$ buildups fit poorly to a single structure with one dipolar coupling. Fitting is therefore done using models with two or more populations each with different couplings. The **closed/semiclosed model** is based on: (1) a single closed structure with associated distances $r_{cG} \equiv$ G16 ^{13}CO-F9 ^{15}N and $r_{cA} \equiv$ A5 ^{13}CO-M17 ^{15}N and corresponding dipolar couplings d_{cG} and d_{cA}; and (2) a single semiclosed structure with distances r_{sG} and r_{sA} and couplings d_{sG} and d_{sA}. Each sample type (HA3fp20 vs HA1fp23 and pH 5 vs pH 7) is a mixture of a closed and semiclosed peptides with respective fractions f_c and $f_s = 1 - f_c$. The f_{c1}, f_{c2}, f_{c3}, and f_{c4} respectively correspond to the HA3fp20/pH 5, HA3fp20/pH 7, HA1fp23/pH 5, and HA1fp23/pH 7 samples. The χ^2 are calculated for an array of d_{cG}, d_{cA}, d_{sG}, d_{sA}, f_{c1}, f_{c2}, f_{c3}, and f_{c4} values with the $(\Delta S/S_0)^{sim}$ for each d calculated by Eq. S11:

$$\chi^2(f_{c1},f_{c2},f_{c3},f_{c4},d_{cG},d_{sG},d_{sA},d_{sG})$$

$$= \sum_{i=1}^{7} \frac{[(\frac{\Delta S}{S_0})_i^{lab} - \{f_{c1} \times (\frac{\Delta S}{S_0})_i^{sim}(d_{cG})\} - (1-f_{c1}) \times (\frac{\Delta S}{S_0})_i^{sim}(d_{sG})]^2}{(\sigma_i^{lab})^2} + \sum_{j=1}^{7} \frac{[(\frac{\Delta S}{S_0})_j^{lab} - \{f_{c2} \times (\frac{\Delta S}{S_0})_j^{sim}(d_{cG})\} - (1-f_{c2}) \times (\frac{\Delta S}{S_0})_j^{sim}(d_{sG})]^2}{(\sigma_j^{lab})^2}$$

$$+ \sum_{k=1}^{7} \frac{[(\frac{\Delta S}{S_0})_k^{lab} - \{f_{c3} \times (\frac{\Delta S}{S_0})_k^{sim}(d_{cG})\} - (1-f_{c3}) \times (\frac{\Delta S}{S_0})_k^{sim}(d_{sG})]^2}{(\sigma_k^{lab})^2} + \sum_{l=1}^{7} \frac{[(\frac{\Delta S}{S_0})_l^{lab} - \{f_{c4} \times (\frac{\Delta S}{S_0})_l^{sim}(d_{cG})\} - (1-f_{c4}) \times (\frac{\Delta S}{S_0})_l^{sim}(d_{sG})]^2}{(\sigma_l^{lab})^2}$$

$$+ \sum_{m=1}^{7} \frac{[(\frac{\Delta S}{S_0})_m^{lab} - \{f_{c1} \times (\frac{\Delta S}{S_0})_m^{sim}(d_{cA})\} - (1-f_{c1}) \times (\frac{\Delta S}{S_0})_m^{sim}(d_{sA})]^2}{(\sigma_m^{lab})^2} + \sum_{n=1}^{7} \frac{[(\frac{\Delta S}{S_0})_n^{lab} - \{f_{c2} \times (\frac{\Delta S}{S_0})_n^{sim}(d_{cA})\} - (1-f_{c2}) \times (\frac{\Delta S}{S_0})_n^{sim}(d_{sA})]^2}{(\sigma_n^{lab})^2}$$

$$+ \sum_{p=1}^{7} \frac{[(\frac{\Delta S}{S_0})_p^{lab} - \{f_{c3} \times (\frac{\Delta S}{S_0})_p^{sim}(d_{cA})\} - (1-f_{c3}) \times (\frac{\Delta S}{S_0})_p^{sim}(d_{sA})]^2}{(\sigma_p^{lab})^2} + \sum_{q=1}^{7} \frac{[(\frac{\Delta S}{S_0})_q^{lab} - \{f_{c4} \times (\frac{\Delta S}{S_0})_q^{sim}(d_{cA})\} - (1-f_{c4}) \times (\frac{\Delta S}{S_0})_q^{sim}(d_{sA})]^2}{(\sigma_q^{lab})^2}$$

Table S4. Best-fit parameters of the closed/semiclosed model [a,b]

HA3fp20 pH 5.0 f_{c1}	HA3fp20 pH 7.0 f_{c2}	HA1fp23 pH 5.0 f_{c3}	HA1fp23 pH 7.0 f_{c4}	d_{cG} - Hz	d_{cA} - Hz	d_{sG} - Hz	d_{sA} - Hz	r_{cG} - Å	r_{cA} - Å	r_{sG} - Å	r_{sA} - Å
0.35(2)	0.55(4)	0.53(3)	0.68(3)	52.1(1.2)	19.5(5)	19.7(6)	5.5(8)	3.89(3)	5.40(5)	5.38(5)	8.25(40)

[a] Fitting is done with the f_c's ≡ fractional populations of closed structure and d 's ≡ dipolar couplings. The corresponding best-fit r's are calculated from the best-fit d 's using r (Å) = [3066/d (Hz)]$^{1/3}$ which reflects a coupling that isn't motionally-averaged.

[b] The fitting is statistically reasonable because χ^2_{min} = 50 is comparable to the number of degrees of fitting = 48. The uncertainty of a best-fit parameter value in parentheses is based on the difference between parameter values for χ^2_{min} + 3 vs χ^2_{min}.

Table S5. ($\Delta S/S_0$) values for d = 51.7 Hz [a]

τ (ms)	($\Delta S/S_0$) Eq. S11	($\Delta S/S_0$) SIMPSON
2	0.011	0.014
8	0.171	0.179
16	0.562	0.570
24	0.913	0.918
32	1.043	1.046
40	0.972	0.978
48	0.866	0.876

[a] This d corresponds to r = 3.90 Å.

[b] The SIMPSON calculation is based on the experimental pulse sequence with input parameters that include the MAS frequency, ^{13}C and ^{15}N pulse fields and durations, and ^{13}CO chemical shift offset and anisotropy.

Each summation is for one buildup with seven dephasing times. The σ^{lab} is the $(\Delta S/S_0)^{lab}$ uncertainty and is calculated using the RMSD spectral noise.[6] The best-fit corresponds to minimum $\chi^2 \equiv \chi^2_{min}$. Table S4 lists the best-fit parameters including uncertainties and χ^2_{min}. The calculated $(\Delta S/S_0)$ values using the analytical expression of Eq. 11 are typically within 0.01 of the values calculated using the SIMPSON program which incorporates the experimental MAS frequency, pulse fields and durations, and chemical shift offsets and anisotropies. Table S5 displays calculated $(\Delta S/S_0)$ from both approaches for d = 51.7 Hz which corresponds to r = 3.90 Å.

12. Alternative fitting models

Fitting was done using alternative models but none of these fittings resulted in χ^2 values as statistically reasonable as the closed/semiclosed model. These fittings are done with the G16/F9 $(\Delta S/S_0)$ buildups because they are significantly larger than the A5/M17 buildups. Fitting is first done with the closed/semiclosed model for the two HA3fp20 buildups and separately for the two HA1fp23 buildups.

The **closed/open model** is based on a single closed structure with r_{cG} and d_{cG} and an open structure which does not contribute to $(\Delta S/S_0)$ because r_{oG} is large and $d_{oG} \approx 0$. The four buildups are fitted simultaneously to the f_c and d_{cG} parameters:

$$\chi^2(f_{c1},f_{c2},f_{c3},f_{c4},d_{cG}) = \sum_{i=1}^{7} \frac{[(\frac{\Delta S}{S_0})_i^{lab} - \{f_{c1} \times (\frac{\Delta S}{S_0})_i^{sim}(d_{cG})\}]^2}{(\sigma_i^{lab})^2} + \sum_{j=1}^{7} \frac{[(\frac{\Delta S}{S_0})_j^{lab} - \{f_{c2} \times (\frac{\Delta S}{S_0})_j^{sim}(d_{cG})\}]^2}{(\sigma_j^{lab})^2}$$
$$+ \sum_{k=1}^{7} \frac{[(\frac{\Delta S}{S_0})_k^{lab} - \{f_{c3} \times (\frac{\Delta S}{S_0})_k^{sim}(d_{cG})\}]^2}{(\sigma_k^{lab})^2} + \sum_{l=1}^{7} \frac{[(\frac{\Delta S}{S_0})_l^{lab} - \{f_{c4} \times (\frac{\Delta S}{S_0})_l^{sim}(d_{cG})\}]^2}{(\sigma_l^{lab})^2} \quad \text{-S26}$$

The **closed/semiclosed/open model** is based on earlier studies interpreted to support ~0.2 fraction of open structure at low pH.[11,12] The two pH 5 buildups are fitted with a 0.2 fraction open structure:

$$\chi^2\{f_{c1},f_{c3},d_{cG},d_{sG}\} = \sum_{i=1}^{7} \frac{[(\frac{\Delta S}{S_0})_i^{lab} - f_{c1}\times(\frac{\Delta S}{S_0})_i^{sim}\{d_{cG}\} - (0.8-f_{c1})\times(\frac{\Delta S}{S_0})_i^{sim}\{d_{sG}\} - 0.2\times(\frac{\Delta S}{S_0})_i^{sim}\{d_{oG}\}]}{(\sigma_i^{lab})^2}$$
$$+ \sum_{k=1}^{7} \frac{[(\frac{\Delta S}{S_0})_k^{lab} - f_{c3}\times(\frac{\Delta S}{S_0})_k^{sim}\{d_{cG}\} - (0.8-f_{c3})\times(\frac{\Delta S}{S_0})_k^{sim}\{d_{sG}\} - 0.2\times(\frac{\Delta S}{S_0})_k^{sim}\{d_{oG}\}]}{(\sigma_k^{lab})^2} \quad \text{-S27}$$

Fitting is done with r_{oG} = 11.5 Å and with r_{oG} = 7.2 Å which are respectively for the open structure of HA3fp20 in detergent and membranes. The membrane structure is the *N*-helix from residues 1-10, *C*-helix from residues 13-20, and turn determined using the ^{13}C shifts of a minor set of E11 inter-residue crosspeaks.[11] Fitting is done for an array of either d_{cG}, d_{sG}, and f_c values or only f_c values with fixed d_{cG}, d_{sG}, and d_{oG} derived from structures of HAfp in detergent and membranes.

Table S6 lists the best-fit parameters of the different models and Figs. S4-S6 display plots of experimental and best-fit $(\Delta S)/S_0$.

Table S6. Best-fit parameters of the models used to fit the G16/F9 SSNMR REDOR data [a,b]

Model	HA3fp20 pH 5.0 f_{c1}	HA3fp20 pH 7.0 f_{c2}	HA1fp23 pH 5.0 f_{c3}	HA1fp23 pH 7.0 f_{c4}	d_{cG} - Hz (r_{cG} - Å)	d_{sG} - Hz (r_{cG} -Å)	χ^2_{min}	deg. of freedom ν_f
Closed/semiclosed								
Simultaneous fit	0.36	0.55	0.53	0.68	52.1 (3.89)	19.2 (5.42)	34	22
HA3fp20 fit	0.33	0.53			56.8 (3.78)	20.2 (5.33)	15	10
HA1fp23 fit			0.51	0.66	55.0 (3.82)	20.7 (5.29)	19	10
Closed/open	0.60	0.78	0.71	0.90	47.9 (4.00)		142	23
Closed/semiclosed/open								
d_{oG} (r_{oG}) = 2.0 Hz (11.5 Å)	0.58		0.68		43.2 (4.14)	18.1 (5.14)	92	10
d_{oG} (r_{oG}) = 8.2 Hz (7.2 Å)	0.51		0.61		41.4 (4.20)	21.8 (5.20)	77	10
d_{cG} (r_{cG}) = 51.7 Hz (3.9 Å) d_{sG} (r_{sG}) = 18.4 Hz (5.5 Å) d_{oG} (r_{oG}) = 2.0 Hz (11.5 Å)	0.47		0.62				137	12
d_{cG} (r_{cG}) =51.7 Hz (3.9 Å) d_{sG} (r_{sG}) = 18.4 Hz (5.5 Å) d_{oG} (r_{oG}) = 8.2 Hz (7.2 Å)	0.44		0.60				83	12

[a] Fitting parameters include $d_G(r_G) \equiv$ dipolar coupling (G16 ^{13}CO-F9 ^{15}N distance) and $f \equiv$ mole fraction.
[b] The typical χ^2_{min}+2-based parameter uncertainties for the closed/semiclosed model are: f, 0.03; and $d_G(r_G)$, 1 Hz (0.02 Å).

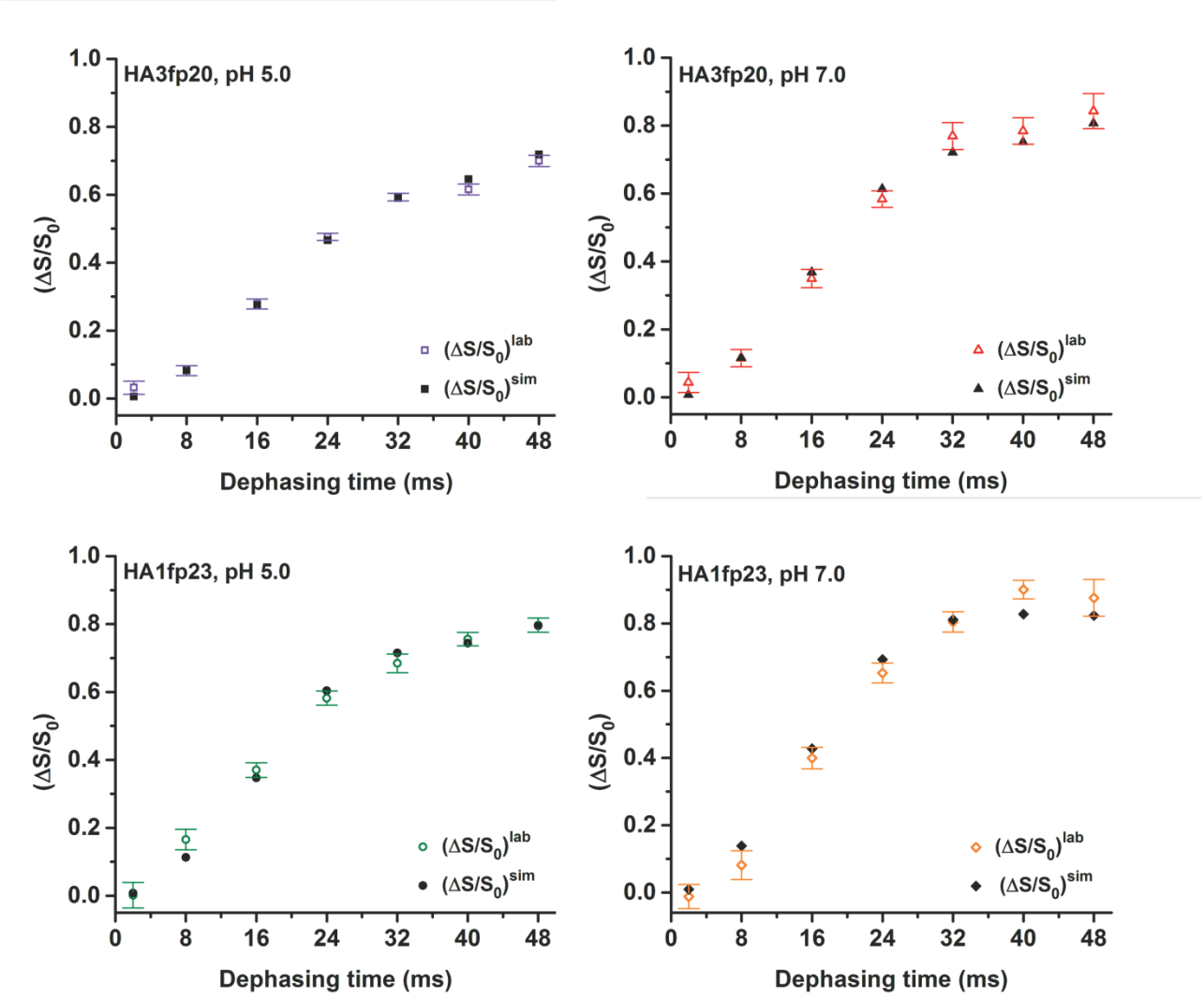

Figure S4. Plots of experimental G16/F9 and best-fit ($\Delta S/S_0$) from the closed/semiclosed model. The HA3fp20 (top) and HA1fp23 (bottom) data are fitted separately.

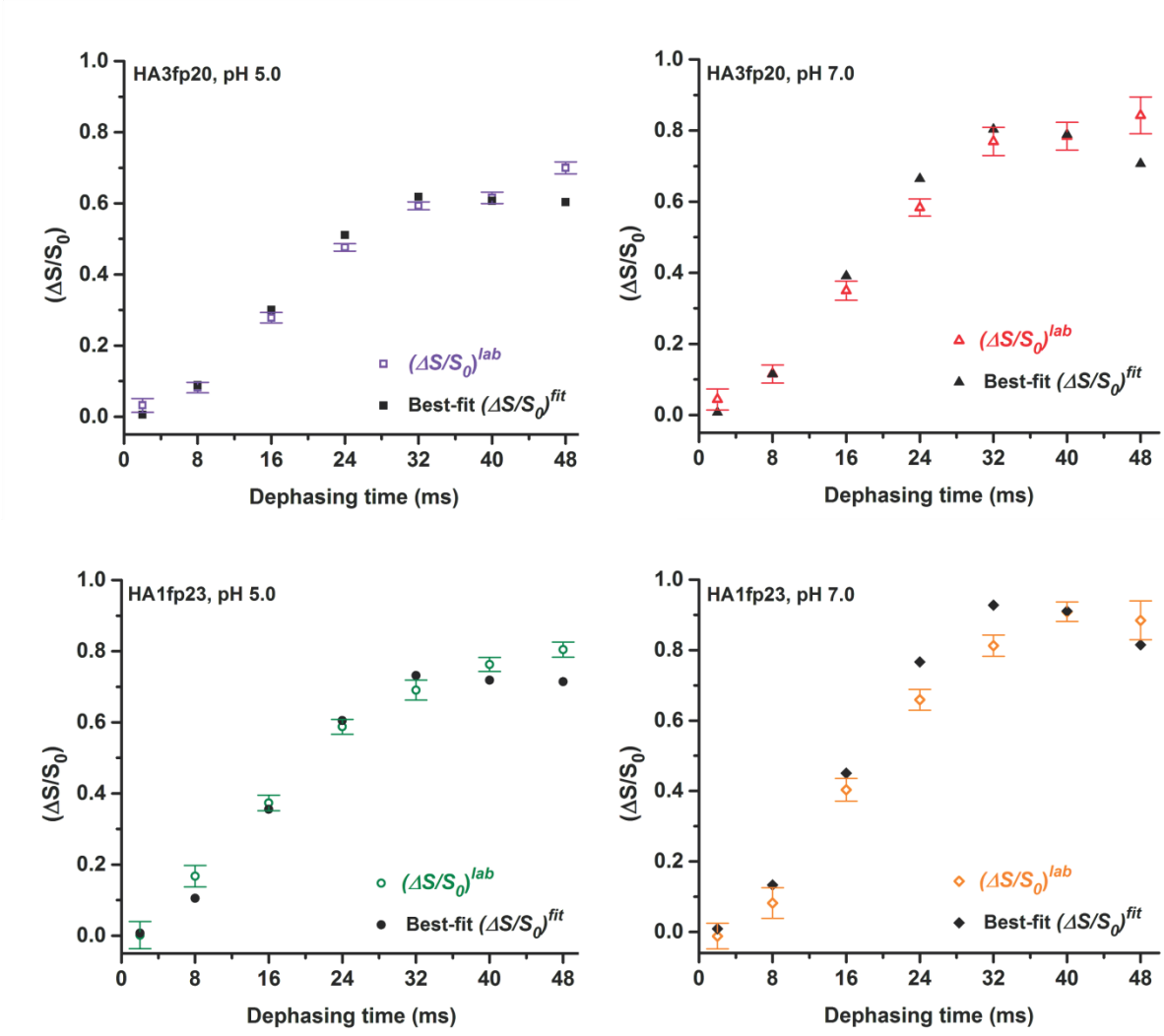

Figure S5. Plots of experimentally-derived G16/F9 $(\Delta S/S_0)^{lab}$ and best-fit $(\Delta S/S_0)$ from the closed/open model.

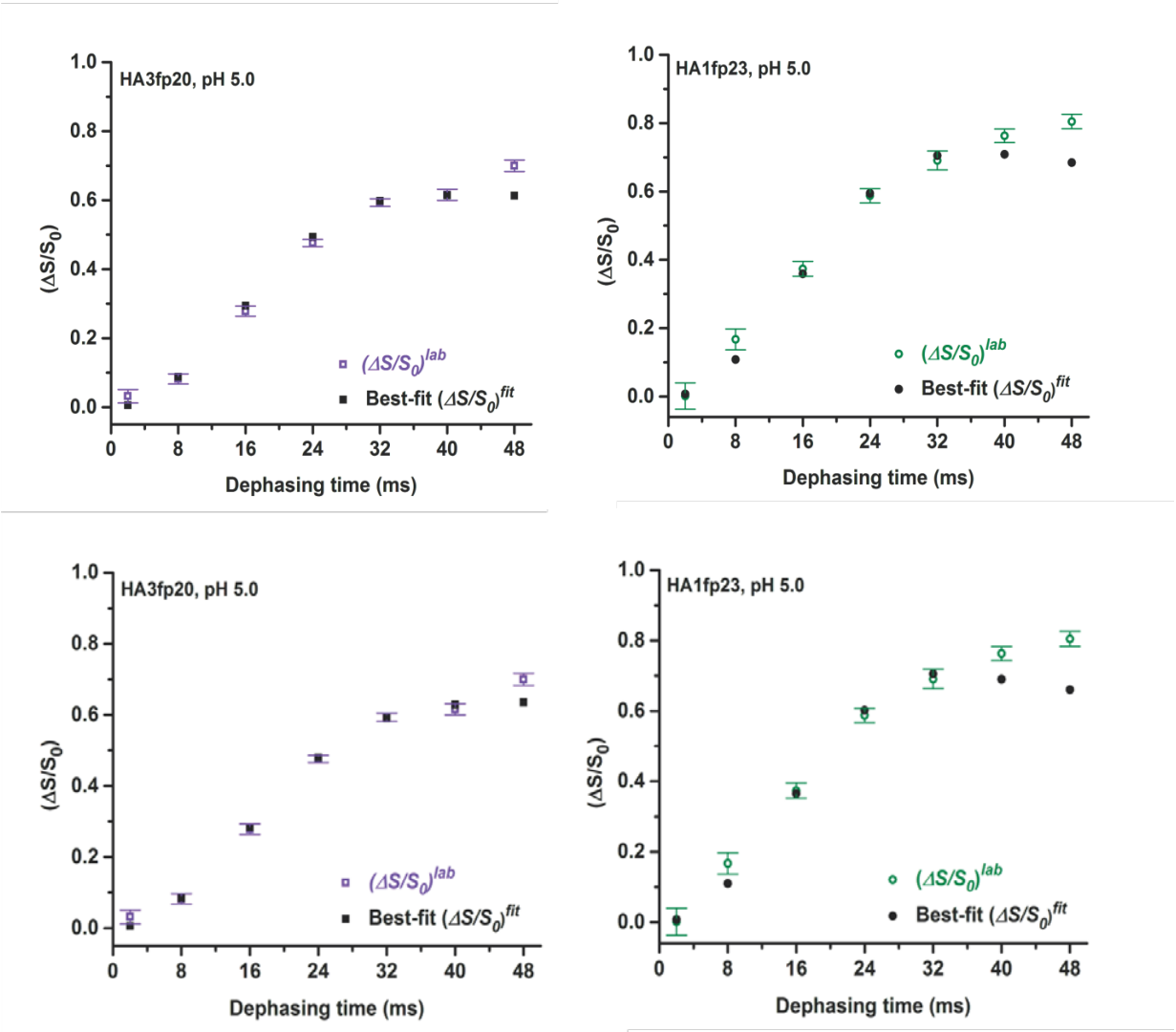

Figure S6. Plots of experimentally-derived G16/F9 $(\Delta S/S_0)^{lab}$ and best-fit $(\Delta S/S_0)$ from the closed/semiclosed/open model using (top) d_{oG} (r_{oG}) = 2.0 Hz (11.5 Å) and (bottom) d_{oG} (r_{oG}) = 8.2 Hz (7.2 Å). The d_{cG} and d_{sG} are fixed.

The fittings yield $r_{cG} \approx 3.9$ Å and $r_{sG} \approx 5.4$ Å that are consistent with earlier structures in detergent and membranes. Because $(\Delta S/S_0)^{open} \approx 0$, the models that include open structure result in a greater fraction closed structure relative to the closed/semiclosed model. The lowest χ^2_{min} is obtained for the closed/semiclosed model and this model is also statistically reasonable based on χ^2_{min} close to ν_f. Much higher χ^2_{min}'s are obtained for the other models that include open structure and the $\chi^2_{min} >> \nu_f$. The closed/semiclosed model is therefore considered most likely.

Very similar best-fit parameters are obtained for simultaneous fitting of all buildups and for separate fittings of the HA3fp20 and HA1fp23 buildups. This supports the hypothesis of a single closed structure and a single semiclosed structure common to both peptides.

13. Buildups at different temperatures

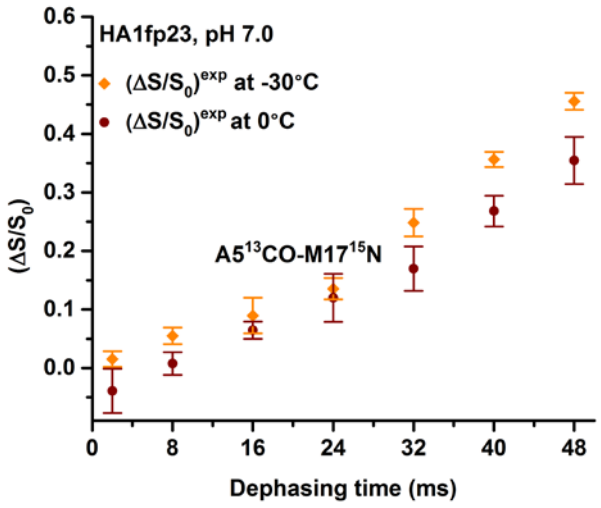

Figure S7. ^{13}CO-^{15}N $(\Delta S/S_0)^{exp}$ buildups with sample temperatures of ~ –30 and ~ 0 ^{o}C (cooling gas temperatures of –50 and – 20 ^{o}C, respectively). The signal-per ^{13}C nucleus-per scan at 0 ^{o}C is about half that at –30 ^{o}C.

13. ^{13}CO-^{2}H fitting. Fig. S8 displays fitting of the $(\Delta S/S_0)^{exp}$ buildup of HA3fp20 at pH 5 with G16 ^{13}CO and F9 ring ^{2}H labeling. The fitting model is: (1) closed and semiclosed structures with f_c = 0.35 and f_s = 0.65 (Table S4); (2) ^{13}CO-^{2}H $d_{cD} \approx 0$ that reflects $r_{CD} > 8$ Å in the closed structure because the F9 ring points away from the *C*-helix; and (3) fitting parameter d_{sD} that reflects ^{13}CO-^{2}H proximity in the semiclosed structure because of the F9 ring location in the interhelical space. The buildup of $(\Delta S/S_0)^{exp}$ is fitted to $[0.65 \times (\Delta S/S_0)^{sim}]$ where the $(\Delta S/S_0)^{sim}$ are for isolated ^{13}CO-^{2}H spin pairs with a single value of d_{sD} and the $(\Delta S/S_0)^{sim}$ are calculated using the SIMPSON program which incorporates the 10 kHz MAS frequency, ^{13}C and ^{2}H pulse fields and durations, and ^{13}CO and ^{2}H anisotropies. The best-fit d_{sD} =19(1) Hz corresponds to r_{sD} = 6.2(1) Å. The fitting model is semi-quantitative because of uncertainties which include: (1)

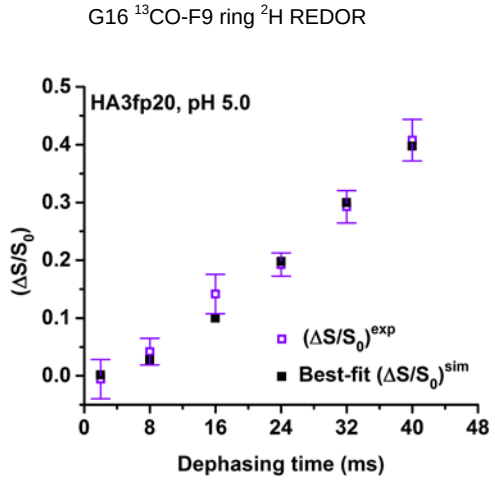

Figure S8. ^{13}CO-^{2}H $(\Delta S/S_0)^{exp}$ and best-fit [0.65 × $(\Delta S/S_0)^{sim}$] buildups with d_{sD} = 19 Hz. The HA3fp20 sample at pH 5 contained G16 ^{13}CO and F9 ring ^{2}H labeling.

five ring ^{2}H's so that the $(\Delta S/S_0)^{exp}$ reflect five somewhat different r_{sD}'s as well as a small contribution from the five different r_{cD}'s; (2) the calculated r_{SD} = 6.2 Å is based on rigid ^{13}CO-^{2}H spin pairs but would be smaller if there were motional averaging of ^{13}CO-^{2}H dipolar coupling from rotation of the F9 ring; and (3) fitting with $(\Delta S/S_0)^{lab}$ rather than $(\Delta S/S_0)^{exp}$ would likely lead to ~20% larger best-fit d_{SD} and ~5% smaller r_{sD} (Table S2).

14. Structural models. The structural pictures are generated using the PYMOL and MOLMOL programs. Table S7 lists the backbone dihedral angles of the closed, semiclosed, and open structural models. NMR data in detergent are the basis for the closed (HA1fp23 at pH 7.4) and open (HA3fp20 at pH 5.0) structures.[13,14] The semiclosed structure is based on SSNMR data of the present and earlier papers for HA3fp20 and HA1fp23 in membranes at pH 5 and 7.[11] The *N*-helix/turn/*C*-helix geometry is similar to the closed structure and the closed structure dihedral angles are used for residues 1-10 and 13-22. The semiclosed residue 11 and 12 angles are based on TALOS analysis of ^{13}C shifts. The semiclosed structure was energy-minimized using the YASARA program.[15] The initial structure was the above backbone with sidechain positions from a MD simulation structure with protonated E11 (F1 structure).[16] The semiclosed backbone was stable under energy minimization and there were small changes in sidechain positions.

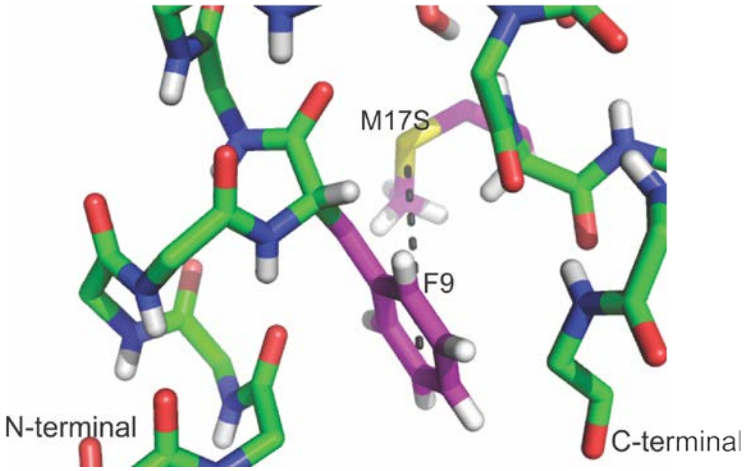

Figure S9. View of the M17 S-F9 ring hydrophobic interaction in the energy-minimized HA3fp20 structure.

Table S7: Backbone dihedral angles of the HAfp structures.

Residue	**Closed/Semiclosed**		**Open**	
	φ	ψ	φ	ψ
G1		-107.8 (97.2)		-160.1 (0.3)
L2	-64.6 (2.3)	-50.6 (2.6)	-46.7 (1.1)	-43.7 (0.1)
F3	-64.2 (0.9)	-46.5 (1.6)	-51.9 (1.6)	-34.9 (0.5)
G4	-56.9 (1.0)	-32.8 (0.8)	-67.6 (0.6)	-34.7 (2.5)
A5	-68.8 (1.3)	-46.4 (0.9)	-72.3 (2.2)	-36.4 (2.6)
I6	-60.9 (0.9)	-52.1 (0.8)	-57.9 (1.1)	-40.6 (1.1)
A7	-65.9 (0.8)	-42.2 (0.4)	-65.6 (1.3)	-35.1 (4.6)
G8	-63.3 (0.5)	-34.8 (0.8)	-53.5 (5.1)	-52.1 (5.7)
F9	-64.8 (0.9)	-44.3 (0.6)	-61.4 (4.6)	-44.2 (4.3)
I10	-66.4 (1.1)	-28.1 (0.9)	-48.7 (3.1)	-32.2 (9.7)

	Closed		**Semiclosed**		**Open**	
	φ	ψ	φ	ψ	φ	ψ
E11	-91.6 (1.2)	-48.4 (1.3)	-69.0 (11.0)	-27.0 (13.0)	-98.3 (12.6)	-2.5 (3.7)
G12/N12	-112.7 (1.2)	-29.3 (1.4)	-96.0 (13.0)	-8.0 (12.0)	-135.5 (23.7)	32.9(37.9)

	Closed/Semiclosed		**Open**	
	φ	ψ	φ	ψ
G13	44.3 (1.0)	-145.6 (1.2)	27.3 (117.5)	5.3 (14.2)
W14	-50.5 (0.4)	-61.4 (1.1)	-39.9 (3.3)	-41.6 (3.5)
T15/E15	-49.3 (0.9)	-33.1 (1.1)	-52.6 (3.8)	-33.2 (4.2)
G16	-69.8 (1.5)	-37.1 (0.6)	-70.2 (5.9)	-18.4 (8.5)
M17	-59.4 (1.2)	-46.7 (2.3)	-97.7 (10.8)	-10.7 (3.6)
I18	-62.4 (0.9)	-50.5 (1.2)	-70.7 (5.5)	-45.6 (8.9)
D19	-53.9 (2.7)	-43.5 (1.7)	-35.9 (44.7)	95.5 (89.7)
G20	-68.1 (2.2)	-34.4 (1.1)	63.1 (64.1)	-41.6 (58.7)
W21	-62.8 (1.3)	-48.8 (2.5)		
Y22	-75.8 (2.7)	-31.3 (2.8)		
G23	47.0 (51.6)	30.1 (86.0)		

15. Hydrophobic Surface Area. The POPS program with 1.4 Å probe radius is used to calculate this area for the closed and semiclosed structures.[17] The hydrophobic surface area of a particular peptide is then calculated as a weighted average using the best-fit f_c and $f_s = 1 - f_c$ of the closed/semiclosed model.

Table S8: Hydrophobic surface areas.

Sample	Area (Å^2)
HA3fp20, pH 7.0	1150
HA3fp20, pH 5.0	1169
HA1fp23, pH 7.0	1298
HA1fp23, pH 5.0	1316

References

(1) Chang, C. D.; Waki, M.; Ahmad, M.; Meienhofer, J.; Lundell, E. O.; Haug, J. D. *Int. J. Peptide Protein Research* **1980**, *15*, 59.
(2) Lapatsanis, L.; Milias, G.; Froussios, K.; Kolovos, M. *Synthesis* **1983**, *8*, 671.
(3) Worman, H. J.; Brasitus, T. A.; Dudeja, P. K.; Fozzard, H. A.; Field, M. *Biochemistry* **1986**, *25*, 1549.
(4) Struck, D. K.; Hoekstra, D.; Pagano, R. E. *Biochemistry* **1981**, *20*, 4093.
(5) Gullion, T.; Schaefer, J. *J. Magn. Reson.* **1989**, *81*, 196.
(6) Zheng, Z.; Yang, R.; Bodner, M. L.; Weliky, D. P. *Biochemistry* **2006**, *45*, 12960.
(7) Gullion, T.; Baker, D. B.; Conradi, M. S. *J. Magn. Reson.* **1990**, *89*, 479.
(8) Morcombe, C. R.; Zilm, K. W. *J. Magn. Reson.* **2003**, *162*, 479.
(9) Zhang, H. Y.; Neal, S.; Wishart, D. S. *J. Biomol. NMR* **2003**, *25*, 173.
(10) Mueller, K. T. *J. Magn. Reson. Ser. A* **1995**, *113*, 81.
(11) Sun, Y.; Weliky, D. P. *J. Am. Chem. Soc.* **2009**, *131*, 13228.
(12) Lorieau, J. L.; Louis, J. M.; Schwieters, C. D.; Bax, A. *Proc. Natl. Acad. Sci. U.S.A.* **2012**, *109*, 19994.
(13) Han, X.; Bushweller, J. H.; Cafiso, D. S.; Tamm, L. K. *Nature Struct. Biol.* **2001**, *8*, 715.
(14) Lorieau, J. L.; Louis, J. M.; Bax, A. *Proc. Natl. Acad. Sci. U.S.A.* **2010**, *107*, 11341.
(15) Krieger, E.; Joo, K.; Lee, J.; Lee, J.; Raman, S.; Thompson, J.; Tyka, M.; Baker, D.; Karplus, K. *Prot. Struct. Funct. Bioinf.* **2009**, *77*, 114.
(16) Panahi, A.; Feig, M. *J. Phys. Chem. B* **2010**, *114*, 1407.
(17) Cavallo, L.; Kleinjung, J.; Fraternali, F. *Nucleic Acids Res.* **2003**, *31*, 3364.